

# Search for transiting exoplanets in globular clusters

*Oskar Nilsson*

---

Division of Astrophysics  
Department of Physics  
Lund University



2023-EXA217

Degree project of 15 higher education credits  
January 2023

Supervisors:  
Jens Hoeijmakers & Anna Arnadottir

Division of Astrophysics  
Department of Physics  
Box 43  
SE-221 00 Lund  
Sweden

## Abstract

This project consists of a transit search in the Messier 3 Globular cluster with the goal to assess the difficulties of observing planetary transits in globular clusters. M3 was observed for a short period of time and by performing PSF fitting, flux measurements could be done to extract light curves of the 290 stars that are included in this project. To determine the stellar type, an HR-diagram was done by observing the cluster with a  $g$  and  $r$  filter on the telescope. The results confirmed the hypothesis that the center of the cluster is too crowded so that no light curves could be extracted. However, at some distance from the center, a transiting Hot Jupiter with radius  $1R_J$  could be readily visible around 90% of the Main Sequence stars in the cluster. At this distance from the center, reliable light curves could be extracted around other types of stars as well. However, due to the big stellar radius of the Subgiant and Giant stars compared to the planetary radius, the transit depth was too small in order to be readily visible in the light curves due to noise. My result points towards an absence of exoplanets in Globular Clusters. This is because the results show a lot of stars where a planetary transit would be easy to detect, thus they could have been detected in previous transit searches done by researchers that had more time and used a better observational setup.



## Populärvetenskaplig beskrivning

Vi hittar planeter överallt vi tittar i Vintergatan. De ser olika ut var man än kollar. Men det finns några platser där planeter verkar vara obefintliga: i klotformiga stjärnhopar. Dessa innehåller hundratusentals stjärnor som, på grund av gravitation emellan dem, hålls ihop och bildar ett stjärnsystem som sträcker sig över hundratals ljusår i diameter. Än så länge har bara en exoplanet hittats i ett klotformig stjärnhop och anledningen till att bara en har hittats är ännu inte fastställd. På grund av det stora antalet stjärnor i dessa "små" system är densiteten hög, vilket gör det mycket svårt att observera individuella stjärnor. Dåliga observationsinstrument, där stjärnor inte kan observeras individuellt, kan vara anledningen till att enbart en planet har hittats, men kanske att exoplaneter här är väldigt sällsynta. Resultatet av min forskning kommer inte bara att ge mer kunskap om vad vi vet om exoplanetpopulationen i stjärnhopar, utan också hur klotformiga stjärnhopar beter sig och vad som pågår inuti dem. På grund av den ökande luminositeten när man närmar sig centrum av stjärnhopen har vi stora begränsningar för att observera exoplaneterna. Och som sagt tidigare: planeter förväntas finnas överallt i universum runt nästan varje stjärna. Så vad skulle vara anledningen till att de inte har upptäckts i en stjärnhop?

För att undersöka denna fråga kommer jag att göra observationer av en klotformig stjärnhop och sedan genomföra mätningar av stjärnornas luminositet för att till slut få fram ljuskurvor som beskriver stjärnornas luminositet över tid. Standardavvikelsen i ljuskurvorna kommer att jämföras med hur mycket stjärnans luminositet minskar när en planet med  $1R_J$  färdas framför stjärnan. Detta förhållande kommer visa för vilka stjärnor som en transit är synlig och inte synlig. Resultatet kommer att beskriva på vilka platser i stjärnhopen som vi har bäst förutsättningar för att observera planeter.

Anledningen till att detta arbete är viktigt är inte bara för att få en klar bild av sammansättningen av ett klotformigt stjärnhop, utan också för att få kunskap om planeter i allmänhet. Om vi skulle hitta planeter i dessa system, skulle de se annorlunda ut? Men huvudsakligen kommer forskningen att ge en tydlig bild av exoplaneters population. Hur planeter beter sig och hur de ser ut baserat på deras miljöer är en viktig del av vår förståelse av livet utanför jorden. Sammanfattningsvis, för att förstå den verkliga naturen hos planeter måste vi känna till deras förekomst i universum, och det är huvudmålet med min forskning.



# Contents

<b>1</b>	<b>Introduction</b>	<b>2</b>
1.1	Theory . . . . .	5
1.1.1	Transit Method . . . . .	5
1.1.2	Globular Clusters & Stars . . . . .	7
1.1.3	Astronomical observations . . . . .	9
<b>2</b>	<b>Data reduction</b>	<b>12</b>
<b>3</b>	<b>Data analysis</b>	<b>25</b>
<b>4</b>	<b>Results</b>	<b>29</b>
4.1	Discussion . . . . .	31
4.2	Conclusion & Outlook . . . . .	34

# Chapter 1

## Introduction

It is thought that every star in our galaxy is likely to host at least one planet<sup>1</sup>. Since 1992, over 5300 exoplanets have been found in the Milky Way and the number keeps growing<sup>2</sup>. But in globular clusters (GC), only one planet has been found<sup>3</sup>. It was found close to the core of the Messier 4 (M4) globular cluster orbiting a pair of pulsar stars and was detected using what is called the pulsar timing method. Pulsar stars emit very precisely timed electromagnetic radiation pulses. The pulsar timing method is used by measuring this radiation and observing regular variations in the pulses periods, which indicates that the star is moving back and forth, orbiting around a common center of mass with another planet. Crowded areas in space, like globular clusters, are contain extreme radiation and gravitational forces and might not seem as an ideal environment for evolution of a planet. As exoplanets are common everywhere in our galaxy, could that not be the case in GCs?

The transit method is a very important tool when searching for exoplanets. Close to 70% of all confirmed exoplanets was first detected using this method<sup>4</sup> and it is done by monitoring the flux of a star over a period of time. By then recording the stellar flux over time, one creates a light curve that shows how the stellar flux varies with time. Detecting periodic fluctuations of the stellar flux in the light curves, can then reveal the presence of an exoplanet due to it partially blocking out light as it orbits in front of the star. Observing individual stars to perform transit detection in GCs can be tricky due to the large number of stars. M4, for example, contains approximately 100 000 stars which, relative to other parts of the universe, all are located close to each other. Because of this, the risk that flux from neighbor stars might interfere, by being included in the light curve, becomes very likely as the center of the cluster is approached and the stellar density increases. Thus one theory to why no exoplanets have been found in GCs is due

---

<sup>1</sup>[solarsystem.nasa.gov/solar-system/beyond/overview/](http://solarsystem.nasa.gov/solar-system/beyond/overview/)

<sup>2</sup>[www.exoplanet.eu](http://www.exoplanet.eu)

<sup>3</sup><https://www.astronomy.com/science/ask-astro-have-there-been-any-exoplanets-discovered-in-globular-star-clusters/>

<sup>4</sup>[www.exoplanet.eu](http://www.exoplanet.eu)



to the crowding resulting in faulty flux measurements of individual stars.

Hot Jupiters (HJ) are gas giants with similar planetary properties as Jupiter. However the orbital distance to their host star is significantly shorter than the Jupiter-Sun distance. This causes HJs to have short orbital periods which makes them easier to detect using the transit method, since they will orbit in front of their host star more frequently. This increases the probability of detecting them, since the host star does not have to be observed for as long to catch a transit. Due to transit geometry, close orbit (0.04-0.05 AU) HJs have a 10% chance of being detected with the transit method given random orbital inclinations, which also contributes to them being found more frequently (National Academies of Sciences & Medicine 2018). The size of HJs are also advantageous when using the transit method since, compared to a smaller planet, more light will be blocked out which will cause deeper light curves where transits are more clearly visible.

R.L Gilliland et al.(2000) carried out a study with the goal of finding HJs (semi-major axis of 0.04-0.05AU) in the 47 Tucane (47 Tuc) GC using the transit method. Using the Hubble Space Telescope (HST), 34000 main sequence (MS) stars were selected to be observed for 8.3 days and used in the survey. MS stars are stars that fuse hydrogen atoms to helium as their primary source of energy. They range from  $\sim 0.1$  up to 200 times the solar mass ( $M_{\odot}$ ). The reason for not searching around stars with larger radius than MS stars (or the very large radius MS stars) is due to the transit depth (the decrease of flux while in transit) would be very small using giant stars, thus detecting a transit is harder. With the knowledge about occurrence rate of transiting HJs at the time, which was about 1%, Gilliland expected to find 17 planets. This number also includes the fact that 10% of all HJ will transit given random inclinations. The result of this survey was that no planets were found, implying that the occurrence rate of short orbit gas giants (HJ) is at least one order magnitude smaller in the 47 Tuc GC than in the solar neighborhood. With more recent knowledge and data, K. Masuda and Winn (2017) reassessed Gillilands paper and found that only  $\sim 2$  planets could have been expected to be found in the 47 Tuc survey. This is because the transiting HJ occurrence rate was revised to 0.4% based on newer Kepler data.

A similar search was performed by J.J.Wallace et al. (2020) in the Messier 4 (M4) GC. The search focused on smaller planets ( $< 0.3R_J$ ) and larger orbital periods (however  $P < 35$  days). Using data from the K2 mission, Wallace extracted 3784 light curves with observation duration of 78 days. 27 potential transits were extracted from the search. However at least 20 were considered false positives, meaning they were not actually transits. The remaining 7 also seemed to be false, as the systematic noise in the data was analyzed.

False positives, in this case, refers to when the light curve show a flux decrease without it actually being a planet in transit causing it. This could be due to other objects passing between the observer and the star. As an example, eclipsing binaries are stars

that move in orbit around each other. Depending on their orientation relative to Earth, one star might block part of the other stars light as a planet would do in transit. This cause for a change in the stellar flux, which at first glance can look like a planetary transit. Other type of noise caused by the telescope such as "bad pixels", which refers to some pixels being more or less sensitive, could also cause measurements to fluctuate. As mentioned, when observing in crowded areas like a GC, it is possible that flux from neighbor stars will more or less interfere with the flux measurement of the star of interest if it is not isolated properly. This could also cause for the light curve to have increasing or decreasing values, if the included flux from the neighboring star is not constant.

Then what are the reasons that exoplanets may be non-existent in GCs? The stars inside of GCs are very old and they have generally lower metallicity compared to the rest of the universe, e.g Chattopadhyay et al. (2021). This is because at the time when they were created, star forming nebulae still consisted mainly of hydrogen and helium, resulting in globular clusters having generally lower metallicity. G. Laughlin (2000) made a study examining the correlation between stellar metallicities and presence of short period planets ( $P < 20$  days). The conclusion was that short orbit planets were more frequently found around stars with higher metallicity than stars with lower. This is because it requires more heavy elements to create a planet. Both Gilliland and Wallace proposed in their work that the low metallicity in both 47 Tuc and M4 ( $[Fe/H]=-0.7$ ,  $[Fe/H]=-1.7$  respectively) is a reasonable explanation for the null result presented in their work.  $[Fe/H]$  is the logarithm of the ratio between the number of iron and hydrogen atoms of a star per unit volume, subtracted by the logarithm of the same ratio of the sun. These conclusions at least agree, with G. Laughlins results and could be an explanation to why there could be at least fewer planets in globular clusters.

Assuming that a GC would contain HJs, would they be located in a specific area of the cluster? A paper published by A.S.Hamers (2017) studying HJs formation in globular clusters, suggested that HJs might be located in the center of the cluster. They discussed that HJs are created at larger radii and by interactions with nearby stars they become excited to high eccentricity orbits. As a result, planets can migrate between host stars more easily, especially in the denser parts of the cluster such as the core. In the outer parts of the cluster, this effect was not seen since it require strong interactions between the planets and stars. This theory came to agree with the location of the one exoplanet found in the M4 globular cluster, which was found close to the center. But as said, the center of a GC is extremely bright and observing individual stars here comes with problems. So this may also be a factor to why no exoplanets have been detected; because it is exceptionally difficult to observe them.

The main goal of this project is to determine transit detection efficiencies at various places around the Messier 3 (M3) GC. It will be done by observing the cluster and injecting (HJ) and simulating planetary transits around stars in measured light curves, to

examine if and where inside the cluster planets have the greatest chance of being detected. This project will be similar to Gilliland and Wallace work in the sense that it will focus on gas giants presence in GCs. This is because they are preferable targets when using the transit method, due to their size relative to the host stars. Since only one exoplanet has been detected in a GC, this project will contribute to more knowledge about the practical difficulties of observing transiting exoplanets in GCs. The project will also contribute with strategies on how to isolate stars to obtain accurate flux measurements in a GC.

## 1.1 Theory

### 1.1.1 Transit Method

When using the transit method to search for an exoplanet, one studies the flux decrease of a star. If a planet were to be in orbit in front of its host star, an observer would detect periodic fluctuations of the stellar flux, visualized in figure 1.1. Assuming the luminosity of the star is homogeneous across its entire surface, the ratio between the flux decrease caused by the planet and the total flux of the star with no transit is equal to the ratio between the planetary and stellar radius squared.

$$\frac{\Delta F}{F_{notransit}} = \frac{R_p^2}{R_*^2} \quad (1.1)$$

Where  $\Delta F$  and  $F_{notransit}$  is the difference in flux during transit and flux outside of transit respectively.  $R_p$  is the planetary radius and  $R_*$  is the radius of the star.

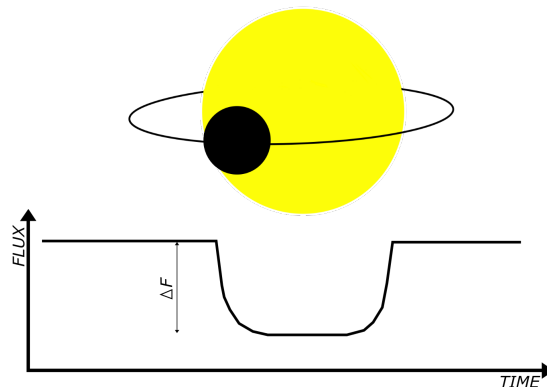


Figure 1.1: Schematic picture of a planet transiting its host star. Also displayed is an example of a light curve representing the stellar flux over time.

The impact parameter  $b$  is defined as the vertical distance between the center of star and center of the planet mid-transit. Impact parameter is a unit less number between 0 and

1, depending on whether the planet is close to the center or the edges respectively. It is calculated using equation 1.2 below

$$b = \frac{a \cdot \cos i}{R_*} \quad (1.2)$$

where  $a$  is the semi-major axis and  $i$  is the inclination of the orbit of the planet. The parameters used in equation 2 are visualized in figure 1.2. Using the impact parameter, the length  $l$  that the planet will travel in transit can be calculated using equation 1.3.

$$l = 4\sqrt{(R_* + R_p)^2 - (bR_*)^2} \quad (1.3)$$

From equation 1.3 it can be seen that for  $b = 0$ , the length and also the transit duration are maximal.

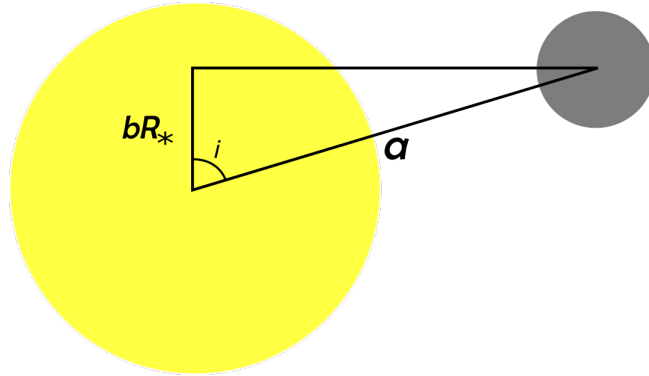


Figure 1.2: Schematic model to visualize the parameters used in equation 1.2.

To be able to detect a planet using the transit method, stars will usually have to be observed for long periods of time. Planets with short orbital periods are thus more efficiently detected, since transits will occur more frequently. HJs are in that way not only preferred because of the close orbit, but also the large size of the planet causes more light from the host star to be blocked out which results in deeper transit light curves, Wallace et al.(2020).

Measurements are done by calculating the total stellar flux of the star over a series of time. To obtain reliable flux values, it is important that the star is isolated. That means that no light from another sources, such as a neighbor star, is included in the measurements. If this were to be the case, one can obtain "false positives" which is flux variations in the light curve caused not by a transiting planet. This is a very possible outcome when doing measurements in a GC since a lot of stars are located close to each other in the obtained images, especially when approaching the center.

### 1.1.2 Globular Clusters & Stars

A globular cluster is a star system that can contain hundred thousands to millions of stars. GCs have a spherical shape with increasing stellar density as the center is approached. The brightness distribution can be described by equation 1.4 below and is dependent on radial distance from the center of the cluster.

$$f(r) = \frac{f(0)}{\left[1 + \left(\frac{r}{r_c}\right)^2\right]} \quad (1.4)$$

In the equation,  $f(r)$  describes the surface brightness at distance  $r$ ,  $f(0)$  is the brightness in the center of the cluster and  $r_c$  is the characteristic core radius, King (1962). As can be seen in figure 1.3, the center of the GC essentially becomes a homogeneous area of bright light, where trying to isolate light from an individual star is not possible using most telescopes.

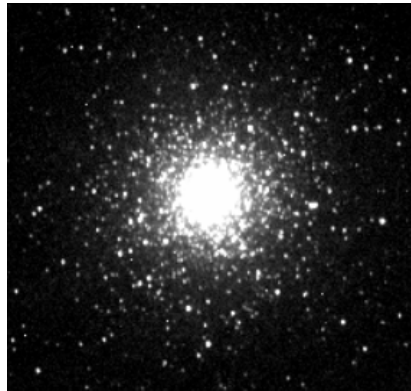


Figure 1.3: The M3 globular cluster. The image is taken by myself during observation with the Stone Edge Observatory (SEO) telescope February 1st 2023.

To be able to determine the stellar properties of the stars that is being observed in a globular cluster, one can create a Hertzsprung–Russell-diagram (HR-diagram). This graphically displays stellar luminosity against temperature, spectral type or color. The position of a star in the diagram reveals the stellar evolution stage and distinguishes the stellar type.

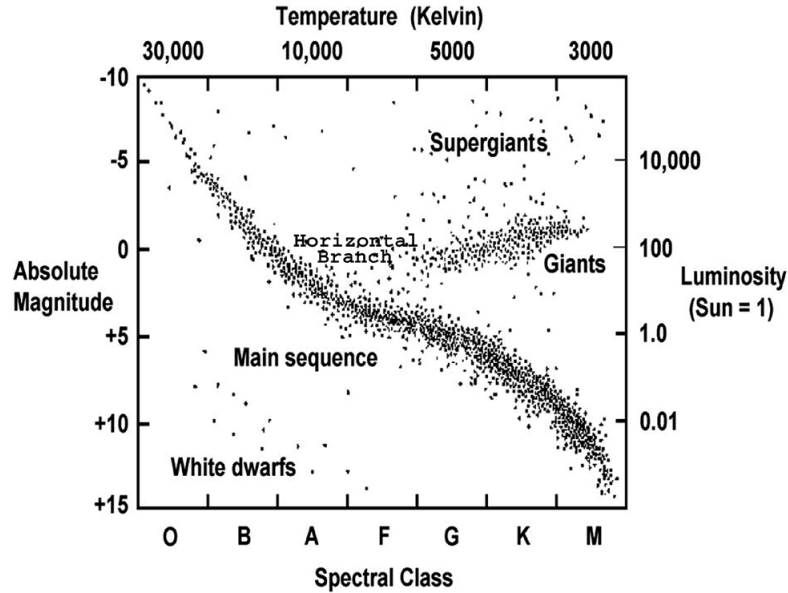


Figure 1.4: An example of a Hertzsprung-Russell-diagram, stars are plotted with luminosity and absolute magnitude against temperature and spectral class. Different branches in the diagram represent different stages in the life of the star. Image taken from [https://chandra.harvard.edu/edu/formal/variable\\_stars/bg\\_info.html](https://chandra.harvard.edu/edu/formal/variable_stars/bg_info.html).

The largest branch seen in figure 1.4 is the main sequence (MS) stars where the Sun is included. The MS contains the stars that burn hydrogen to helium, that is about 90% of stars in the universe. The lower mass MS stars ( $< 8M_{\odot}$ ) will evolve to the giant branch, whereas the higher mass MS stars ( $> 8M_{\odot}$ ) will evolve to the super-giant branch. Main sequence stellar masses,  $M$ , can be approximated to be proportional to their luminosity,  $L$ , as

$$L \propto M^{3.5} \quad (1.5)$$

where they are expressed in solar mass and solar luminosity. From this, the stellar radius can be approximated

$$R_* = R_{\odot} \cdot \left( \frac{M_*}{M_{\odot}} \right) \quad (1.6)$$

where  $R_{\odot}$  and  $M_{\odot}$  are the solar radius and mass respectively. Knowing the luminosity and radius of a main sequence star one can estimate the effective temperature of the star using

$$T_e = \left( \frac{L}{4\pi\sigma R_*^2} \right)^{1/4} \quad (1.7)$$

where  $\sigma$  is the Stefan-Boltzmann constant.

The peak wavelengths of the photons that are emitted by a star are fully dependent on its temperature. This is approximated by Wien's displacement law that relates temperature and wavelength in equation 1.8 below

$$T = \frac{b}{\lambda_{peak}} \quad (1.8)$$

where  $\lambda_{peak}$  is the peak wavelength of the star and  $b$  is the Wien's displacement constant. Hence by observing the spectra of stars, their temperature can be extracted and used to determine the star type in a HR-diagram.

### 1.1.3 Astronomical observations

By observing stars using different filters, the flux emitted at different wavelengths can be extracted. Different types of filters and their properties are listed in table 1.1.

Filter	Filter properties
<b>u (Ultraviolet)</b>	Transmits wavelengths in the violet-ultraviolet range (300-400nm)
<b>g (Green)</b>	Transmits green wavelengths (400-550 nm)
<b>r (Red)</b>	Transmit red wavelengths (550-700 nm)
<b>i (Near infrared)</b>	Transmit the near infrared wavelengths (700-800 nm)
<b>z (Infrared)</b>	Transmit the infrared wavelengths (>800 nm)

Table 1.1: Different filters and their properties in the SDSS photometric system.

This means that observing with the g filter, for example, will cause photons with wavelengths representing green light to be transmitted through the filter. Whereas photons with shorter wavelengths will not be transmitted as well. This implies that hot stars, that emit more photons representing green/blue light, will appear brighter in the image compared to the colder stars that emit photons representing more red light. That is, the hotter stars will have a greater magnitudes than the colder stars when observing with the g-filter. By then subtracting these magnitudes by the magnitude of the same stars observed with the r filter, one get what is called color (g-r). The magnitude of the stars are dependent of their temperature and can be used in an HR-diagram instead of plotting temperature, as color and temperature are related. An example of a color diagram is shown in figure 1.5 below.

Features of a globular cluster H-R diagram (M3).

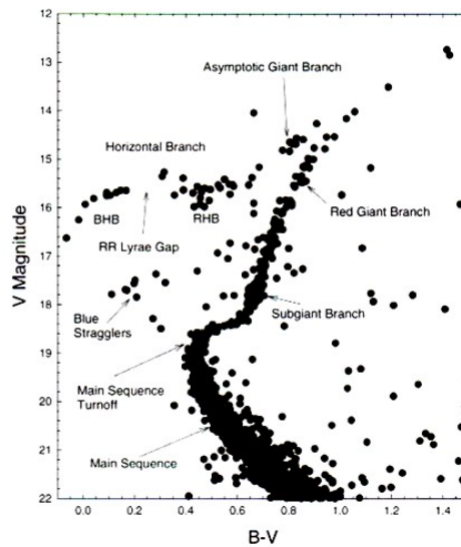


Figure 1.5: HR colour diagram of the stars in the M3 globular cluster. This diagram uses the Johnson filter system that contains B (blue) and V (visible) filter. However the principles are the same as for the SDSS system. Credits: Oliver Young <sup>6</sup>

When using any optical system, light diffraction will occur. A star will emit photons in every direction. When the photons approach the opening of the telescope aperture, light towards the edges will be spread out as displayed in figure 1.6. This is what causes stars to appear "blurry" towards their edges which also can be seen in figure 1.6.

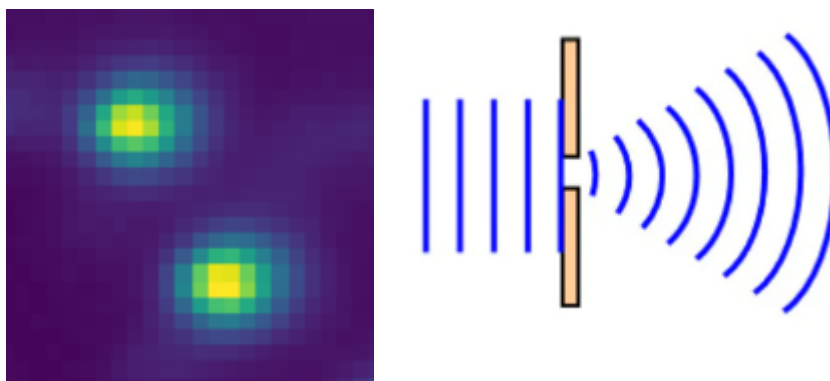


Figure 1.6: Left: Visual representation of two point sources where light diffraction causes the sources to appear blurry. The figure is a sub image of one image taken of the M3 GC during the observations February 1st 2023. Right: Visual representation of light diffraction.<sup>8</sup>

<sup>6</sup><https://slideplayer.com/slide/8572146/>



Though the left figure in 1.6 represents two stars that are point source objects, they are rather manifested as discs with increasing intensity as the center is approached. This is referred to as a Point Spread Function (PSF) and describes the spread of any point source observed by a telescope. In this project PSF will be approximated by fitting a 2D Gaussian to the source. In reality, this effect is seen as an airy pattern around the source, that is rings with decreasing intensity as the distance from the center become larger. The intensity of the source is normal distributed, thus why a Gaussian fit is used as approximation.

When using a telescope, the diffraction effect can cause close adjacent stars to not be individually resolved. The Rayleigh criterion (equation 1.9) describes the minimum angular distance that two stars need to be separated to be individually resolved,

$$\theta = 1.22 \frac{\lambda}{D} \quad (1.9)$$

where  $\theta$  is the angular resolution expressed in radians,  $\lambda$  is the wavelength of the light and  $D$  is the diameter of the telescope lens aperture. This effect can be seen in figure 1.3 where, as the center is approached, individual stars can no longer be individually resolved since they are too close to each other.

---

<sup>8</sup><https://scienceready.com.au/pages/diffraction>

# Chapter 2

## Data reduction

Observations were done using the Stone Edge Observatory (SEO) 0.5m telescope located in Sonoma, California. SEO is privately owned and is operated by the University of Chicago, and through them students and educators can apply for time on the telescope. Using the messaging software Slack <sup>1</sup> the telescope could be controlled by myself in Lund, Sweden. The observation lasted approximately 4 hours between 3pm and 7pm local time in California February 1st 2023. Figure 2.1 below displays the "Clear Sky Chart" of the weather conditions during the night of observation. As can be seen, little to no clouds were present during the observations.

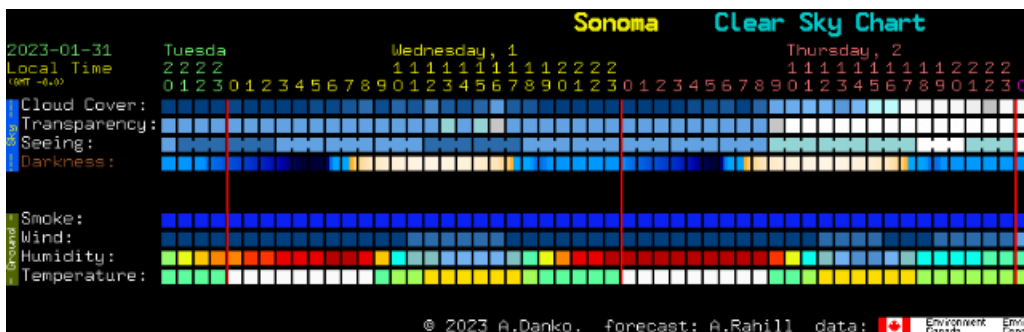


Figure 2.1: Sky chart of the night of observation. Image obtained from "cleardark-sky.com" via the "/sky" command in Slack. Looking at "Cloud Cover", blue represents no clouds and white represent clouds.

After testing capturing frames with different exposure times, that is for how long the camera should collect photons, it was established that 180 seconds was the best since a greater time would increase the risk of brighter stars being over exposed. During the 4 hours of observation, 63 science images of the M3 globular cluster were captured each with an exposure time of 180 seconds with no filter.

<sup>1</sup>www.slack.com

To obtain images with minimal amount of noise, one will have to preform corrections on the images taken. It works by taking calibration frames containing noise that later can be subtracted from the raw science images. When working with astronomical images there are typically three different types of frames one collects to minimise the noise: bias, dark and flat frames.

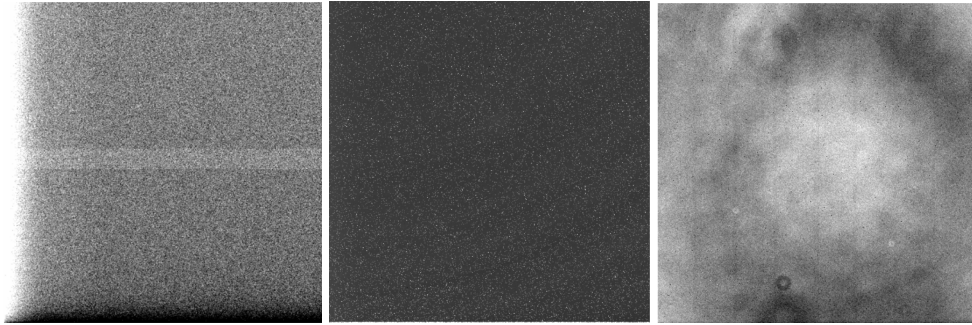


Figure 2.2: Example of master bias, dark and flat frames. The master frames was created from frames obtained during the observation done 1 February with the SEO telescope located in Sonoma, California.

A detector will typically produce a small positive reading for each pixel that is called the bias. Bias frames are obtained by taking zero exposure time images with the shutter closed. By collecting several bias frames one can create a master bias frame. The master bias contains the average signal of several bias frames. This frame is then subtracted from all the raw science images.

Dark frames capture the thermal electronic noise that is caused by temperature differences when taking long exposure images. By taking equally long exposure picture with the shutter closed, this random noise will be captured. Multiple dark frames are then averaged, to create a master dark frame which then is subtracted from all the raw science images in order to remove the noise.

Flat frames are taken to make every pixel give the same value when exposed to the same quantity of light. Lens dust and vignetting effects are factors that can block out light before it is captured by the camera, causing some pixels to have lower counts than they really should have. To capture these differences, the telescope is unfocused and pointed to a field as uniform as possible to make sure every pixel is exposed to equal quantity of light. A master flat frame is created by taking the median of all the flat frames. The raw science images are then divided by this master flat frame to get rid of pixel-to-pixel variations, McLean (2008). The result of subtracting the master bias, dark and dividing the flat frames were images with significantly less noise than the raw science images.

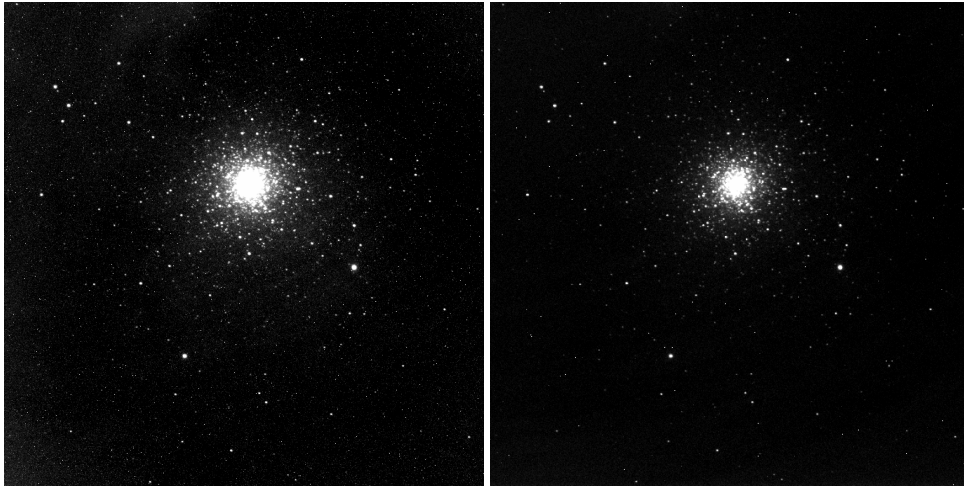


Figure 2.3: Image of the M3 cluster before (left) and after (right) image reduction. Images obtained during the observation run on February 1st with the Stone Edge Observatory telescope located in Sonoma California. Both images is displayed with the same color scale and limits.

Both bias and dark frames were taken at random times throughout the observation. Flat frames, on the other hand, were taken at the very end of the observation. This is because you want the field of view to be as uniform as possible, thus the flat frames were taken when the sky became a little bit illuminated by the morning twilight. It also might require moving the telescope, steering away from the stars which would be not so very time efficient to do it while observing the GC. With bias and dark however, the shutter just need to be shut which makes it very easy to capture them without it interfering with where the telescope is directed. In total: 16 bias frames, 13 dark frames and 21 flat frames was captured during the observation. However 6 of the 21 flat frames was considered to be over saturated and not thus usable, which gave 15 frames to make the master flat.



Figure 2.4: Picture of one of the saturated flat frames taken during the observation. Compare to the rightmost image in figure 2.2.

To be able to identify the stars in the noise reduced images, a "star finder algorithm" that detects and labels stars was developed. The program was created using existing packages in python (Mainly: `astropy`<sup>2</sup>, `photutils`<sup>3</sup> and `DAOSStarFinder`<sup>4</sup>) that were adapted to work for my specific needs. The algorithm works by StarfinderDAO searching the images from the observation for pixels with counts above a set threshold value, which indicate the presence of a star. The stars are then assigned a number equal to the order they were detected in the image. The coordinates to where in the picture they were found were then recorded together with the pixel count.

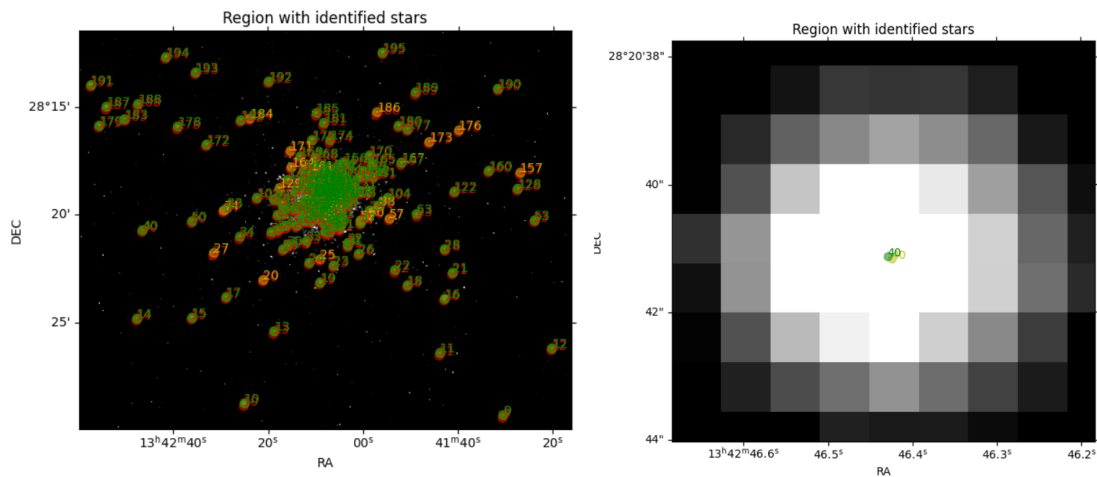


Figure 2.5: A visual representation of the star finder algorithm with threshold value 6000. The red dots indicates the initial position of the star in the first image. The green dots represents the position of the stars in the second picture. The yellow dots are the predicted positions of the green dots. The image to the right shows the accuracy of the predicted shift, where a star is correctly predicted within a single pixel.

Using a threshold value of 6000 counts per pixel, StarfinderDAO was able to identify 195 individual stars in the images. Lowering the threshold value would result in more stars being identified. For example using the threshold value of 3000, StarfinderDAO identified 320 stars. However, lowering the threshold value also increase the risk of noise being identified as a star.

Since the observation was done over several hours there was a small shift between the stars between every image (visualised in figure 2.6), caused by the rotation of the Earth together with the fact that the tracking of the SEO telescope was not perfect. To be able to find and follow the same stars throughout the series of frames, my algorithm predicts the position of every star found in the first image onto any other image later in the se-

<sup>2</sup><https://www.astropy.org/>

<sup>3</sup><https://photutils.readthedocs.io/en/stable/>

<sup>4</sup><https://photutils.readthedocs.io/en/stable/api/photutils.detection.DAOSStarFinder.html>

ries. It does so by calculating the shift of a bright star, which we call the tracking star, between two frames and applying this same shift to every other star found. In this first version of the star finder, this tracking star was chosen to be the first identified star in the image. By then simply subtracting the x and y pixel coordinates of the star in the two frames, the shift in both x and y direction were calculated and applied to every other star identified in the frame. The problem with this version of calculating the shift was that the first identified star would not necessarily be the same in every frame. As can be seen in figure 2.6, a lot more stars are visible in the 34th frame that were not visible in the first frame. This caused this first version of the star finder to only act as a star identifier used only to obtain the positions of stars in the first frame in the series. The method of calculating the shift was later updated when working with tracking the stars over the entire series of frames. With small shifts however (for example between the first and the second frame), this first version calculated shifts with very high accuracy as displayed in figure 2.5. But for it to work for my future needs, a better definition of the tracking star was implemented.

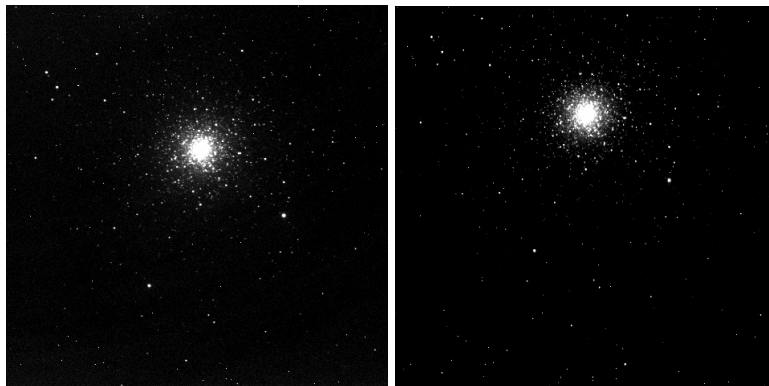


Figure 2.6: Left: The first frame in the series of frames taken during the observation. Right: The 34th frame in the series. When looking at the two images it is clear that the GC shifted upwards in the image as the observation proceeded.

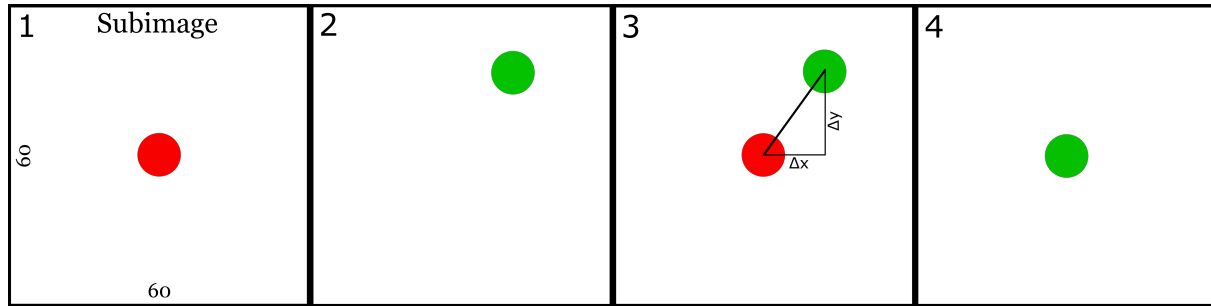


Figure 2.7: Visual representation of how the updated star finder algorithm calculates the shift using a tracking star in a 60x60 pixel sub-image. 1: Tracking star is found in first frame. 2: Tracking star is found in second frame, however it is not centered. 3: The shift is calculated by subtraction of positions in frame 1 and 2. 4: End of iteration, sub image is shifted such that the tracking star is placed in center and the loop starts over.

Figure 2.7 shows a schematic representation of how the new, updated star finder algorithm calculate the shift in two subsequent frames. The problem with the first version was that the tracking star was not explicitly defined. Thus the tracking star was now instead chosen to be a bright star that was visible in every frame and located far outside of the cluster with no other stars in its direct vicinity. In two subsequent frames, a sub image, with size 60x60 pixels, was centered at this tracking star. Within this sub image, StarfinderDAO would find only the tracking star since no other stars would be enclosed. By then simply subtracting the x and y pixel coordinates of the star in the two frames, the shift in both x and y direction were calculated and applied to every other star identified in the whole frame. This allowed for equally accurate predictions but with a guarantee that the tracking star is the same in every frame. At the end of every iteration, the position of the tracking star is updated such that the sub image follows the star through out the entire series. This method however requires that the shift of the star between two subsequent frames is never greater than 30 pixels in any direction.

By knowing the exact positions of the stars and knowing how to track them, the project proceeded by creating light curves of individual stars in the globular cluster. The initial approach was to calculate the stellar flux using a circular aperture that enclosed the star and extracted the total flux. Aperture photometry is a common approach and is used frequently in scientific articles. As an example, Michael E. Higgins (2023) uses this method to analyze TESS data. With this method however, the entire star could not be guaranteed to be enclosed in every image. As displayed in figure 2.8, small discrepancies of the stellar coordinates caused pixels in the outer part of the star to not be included in the aperture; resulting in faulty values of the total flux. Making the aperture bigger would work for stars in the outer parts of the GC where the stellar density is not as great. But when approaching the center, the risk of other stars also being partially included in the aperture became greater as the field becomes more crowded.

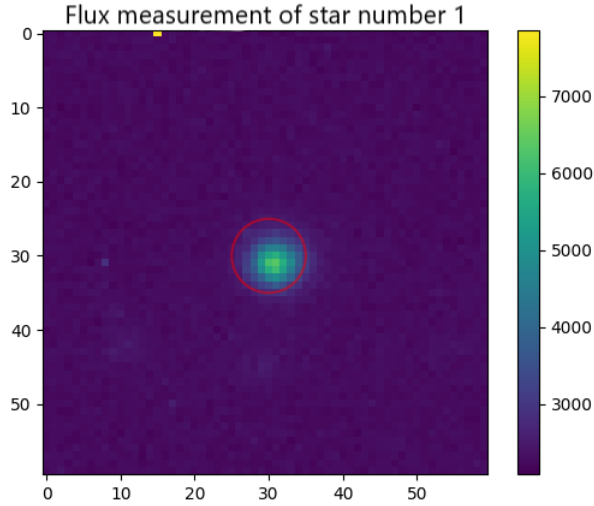


Figure 2.8: Visual representation of how the circular aperture method could cause errors when calculating the stellar flux as the entire star is not fully enclosed by the circle.

Instead of measuring the flux using an aperture, a 2D Gaussian was fitted to the stars instead. The Gaussian fitting process started of by giving the program the x and y coordinates of a star of interest and the tracking star in the first frame in the series. After this the code enters a for loop, looping through all the frames in the series. In the beginning of every iteration the shift is calculated by identifying the position of tracking star in the new frame, as explained. After the shift is calculated, the shift is added to the coordinates of the star of interest, predicting the position of the star in the next frame and extracts a sub image with the star of interest in the center of it. At the end of every iteration, the coordinates of the star of interest and the tracking star are updated by adding the calculated shift to it. Hence the next iteration will begin with calculating the shift between the updated coordinates with the next coming frame and so the loop continue.

Before the sub images are scanned for stars, the sub images are scanned for bad pixels. This include pixels that have produced a signal without there being an actual star. Most of these bad pixels are eliminated in the image reduction but since the noise from both bias and dark are random, there will still be some pixels that survive the reduction. These pixels are called "hot pixels", see figure 2.10, and cause errors in the code since the Gaussian function will try to preform a fit to it. But since the signal is only one pixel, it will often fail. By simply comparing all the pixels in the sub image with their neighboring pixels, such sudden changes in the pixel counts can be identified. The code loops through all pixels in the sub image where for every pixel, the values of its 8 neighboring stars are used to calculate the median absolute deviation (MAD). This method measures the variability of the pixel values. If  $X_i$  is the set of neighboring pixels, let  $\tilde{X}$  be the median of the set:

$$\text{MAD} = \text{median}(|X_i - \tilde{X}|)$$



By then placing the condition that if the center pixel value subtracted by  $\tilde{X}$  is larger than 12 times the MAD value, the center pixel deviates too much from its neighbor pixels and are treated as a hot pixel, and its value is changed to have the same value as  $\tilde{X}$ . In the end of every iteration, when the sub image is plotted, such pixels are marked with a red X as displayed below in figure 2.9.

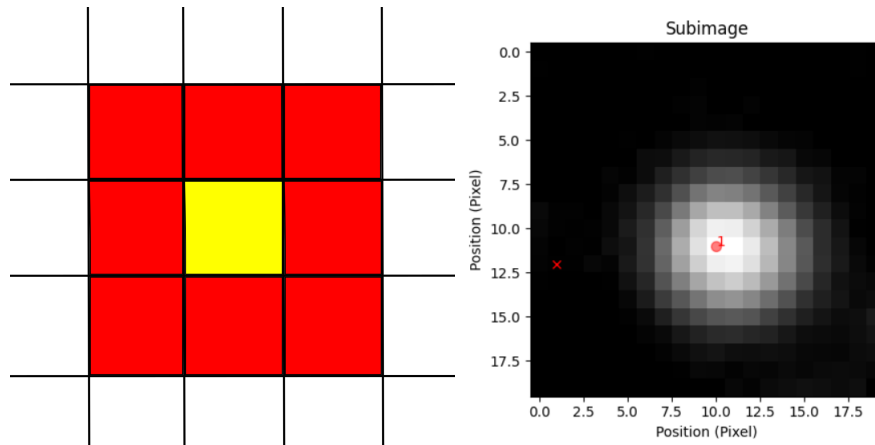


Figure 2.9: Left: Schematic picture of the pixels used in the MAD method. Each box in the figure represent a pixel in the image. Yellow box denotes the target pixel and the red boxes are the neighboring pixels,  $X_i$  that is used to calculate MAD. Right: Plot of a sub image, the red cross located at the left in the image denotes the position of a hot pixel. Picture obtained from the code.

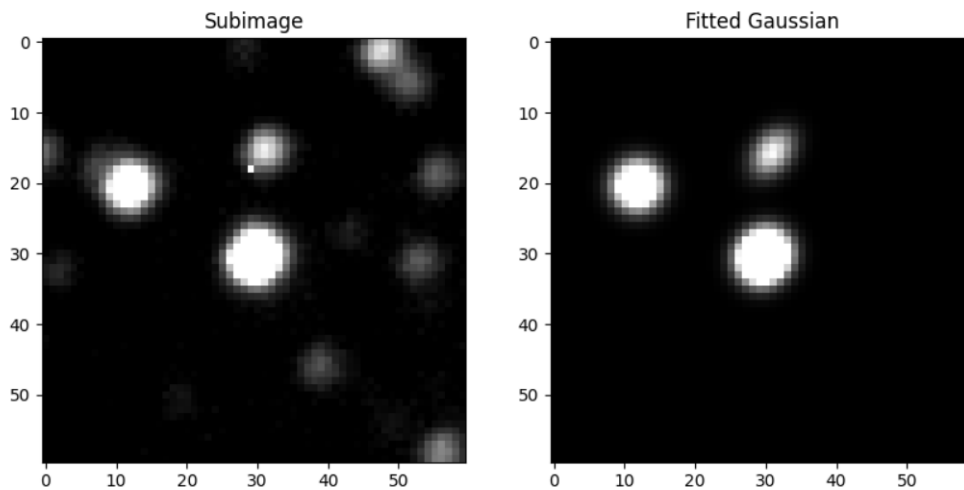


Figure 2.10: Example of how hot pixels can cause errors when fitting. The hot pixel seen at approximately  $(x,y)=(30,18)$  in the left plot, causes the Gaussian fit (right plot) of that star to become elongated.

Inside of the loop, after the shift and MAD calculations, StarfinderDAO searches the sub image for stars. Apart from the star of interest, located in the center of the sub image, neighbor stars will also be detected. StarfinderDAO gives an output including  $x$  and  $y$  position and pixel count. The 2D Gaussian is defined and fitted to all the stars identified by the StarfinderDAO. It starts of by defining the function of the Gaussian as

$$g(x, y) = \sum_1^n \left( \delta + A \cdot \exp \left[ -(a(x - x_n)^2 + 2 \cdot b(x - x_n)(y - y_n) + c(y - y_n)^2) \right] \right) \quad (2.1)$$

Where  $A$  is the amplitude of the Gaussian,  $x_n$  and  $y_n$  are the center coordinates of star  $n$  and  $\delta$  is the offset value, that is the background value and is set to be the mean of the entire sub image region containing the star of interest. Values  $a$ ,  $b$  and  $c$  are defined as

$$\begin{aligned} a &= \left( \frac{\cos^2 \theta}{2\sigma_x^2} \right) + \left( \frac{\sin^2 \theta}{2\sigma_y^2} \right) \\ b &= - \left( \frac{\sin 2\theta}{4\sigma_x^2} \right) + \left( \frac{\sin 2\theta}{4\sigma_y^2} \right) \\ c &= \left( \frac{\sin^2 \theta}{2\sigma_x^2} \right) + \left( \frac{\cos^2 \theta}{2\sigma_y^2} \right) \end{aligned}$$

Here  $\sigma_x$ ,  $\sigma_y$  are the standard deviation in  $x$  and  $y$  direction respectively and  $\theta$  is the rotation angle.

The values for  $x_n$  and  $y_n$  are set to be where the StarfinderDAO finds the stars and the amplitude is set to be the pixel count at  $(x, y)=(x_n, y_n)$ . The values of the parameters are given to the Gaussian function as initial parameters together with guesses for  $\sigma_x$ ,  $\sigma_y$ ,  $\theta$  and offset. The guesses for these parameters was put in myself where  $\sigma_x = 2.5$ ,  $\sigma_y = 2.5$ ,  $\theta = 0$  and offset is set to be the mean of the entire sub image. These guesses were set to be the same for every star.

Using the `scipy.optimize` package, the program automatically adjust the initial guesses and optimize them to obtain a more accurate Gaussian fit to the stars. However, as the crowding became greater and the sub images started to contain many close neighboring stars, the optimizer made a lot of mistakes. As an example, if two stars was overlapping each other in the sub image, StarfinderDAO identified them as two separate stars, however the optimizer saw them as the same star. This caused the optimizer to either give two stars the same  $x$  and  $y$  coordinates or give one of the stars completely different values, which in both cases resulted in faulty Gaussians. An example of this can be seen in figure 2.11. To resolve this problem, the optimizer was given upper and lower boundaries. The StarfinderDAO was very accurate in the vast majority of times, thus

the upper and lower boundaries for  $x_n$  and  $y_n$  was  $\pm 3$  pixels. This means that the optimizer was forced to find the best parameters for the position within 9 pixels of where the StarfinderDAO had identified the star. Similarly,  $\sigma_x$  and  $\sigma_y$  was set to have lower bound of 1.5 and upper of 3, since it was noted that it was between these values the majority of stars were approximated to.

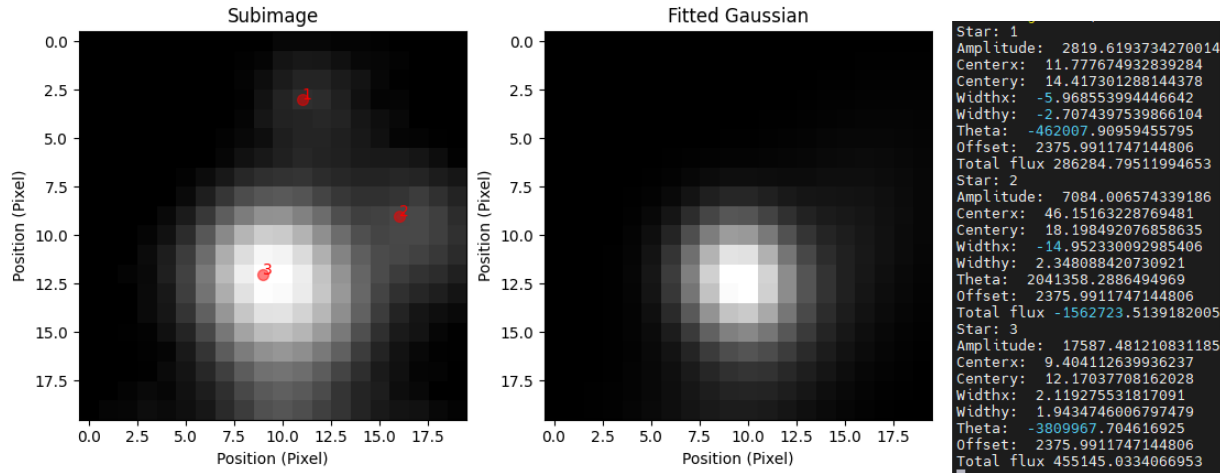


Figure 2.11: An example of the curve fit failing to find the optimized parameters for star number 1 and 2. As can be seen in the "subimage" figure, star number 1 have been detected by StarfinderDAO at  $(x, y) \approx (11, 3)$  and star number 2 at  $(x, y) \approx (16, 9)$ . However, in the print statement it can be seen that the curve fit gave star number 1 and 2 the optimized  $x$  and  $y$  values  $(11, 14)$  and  $(46, 18)$ , which both are very far of from the initial guesses obtained from the StarfinderDAO. As can be seen in the "fitted gaussian" image, neither star number 1 or 2 are fitted in the image. Images obtained from the code output.

For some stars, the optimizer was unable to find a good fit. The curve fit was initially set to only alter the parameters 2800 times and if no optimized parameters was found the algorithm aborted. This was solved by a "try" statement where, after the 2800th iteration the number increased to 10,000 iterations. Still, for some stars, it was unable to find a good fit. Thus after the code has tried 12,800 times, the fitting method are changed from the "Levenberg-Marquardt" method to the "dogbox" method. Both algorithms are used to solve nonlinear least square problems, however dogbox an extension of the Levenberg-Marquardt algorithm, specifically made to handle non-linear least squares problems with bound constraints and by using "dogbox" as the last try resulted in all stars to obtain fitted Gaussians.

The Gaussians are then integrated to obtain the total flux value of each star. The integration was solved analytically by using the formula for a multivariate normal distribution. This solved the general case of a Gaussian with several variables.

$$I = \int \int f(x,y) dx dy = \int \int A \cdot \exp[-((x - x_n)^2 / (2\sigma_x^2) + (y - y_n)^2 / (2\sigma_y^2))] dx dy$$

Solving the integral by integrating over the entire plane gives

$$I = A \cdot 2\pi \cdot \sigma_x \sigma_y$$

The optimized values of the Gaussians are placed in this equation and the total flux of the stars are calculated. All optimized values are then printed in the terminal together with the value of the total flux of the corresponding star. The sub image is then plotted side by side with a Gaussian fit of the sub image. For every frame, the flux of the star of interest is saved in a list. When the loop is finished, these flux values are plotted over time.

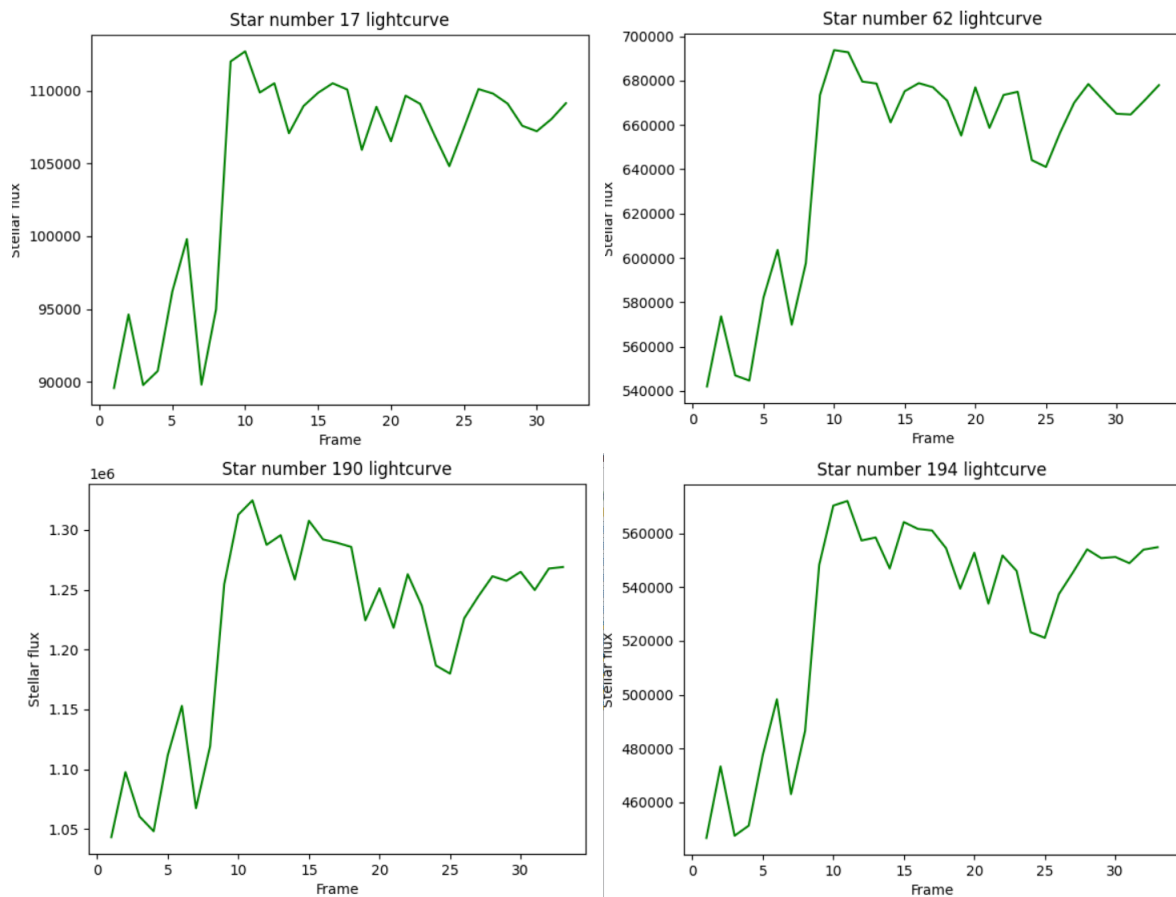


Figure 2.12: Measured stellar flux of stars numbered 17, 62, 190 and 194.

As can be seen in figure 2.12, the flux varies a lot and detecting a transit from these curves would not be possible since there will not be a distinction between this noise

and an actual transit. However, the flux variations are mostly the same for all the stars. They all have the same characteristics since the variations is noise caused by external factors. The 4 stars presented in figure 2.12 are chosen to be reference stars, where the 4 curves are averaged to create an average reference flux measurement. The reference stars was chosen depending on position and brightness. The positions of the reference stars are displayed in figure 2.13 below.

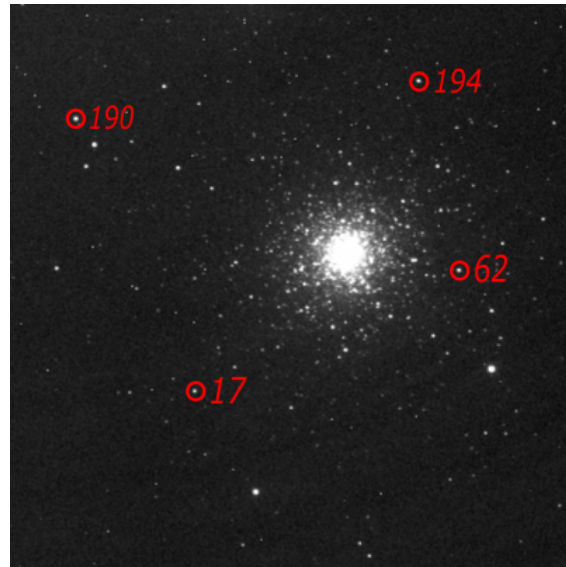


Figure 2.13: Positions of the chosen reference stars 17, 62, 190 and 194. Picture obtained from the observation on 1 February 2023.

As can be seen, they are spread out around the cluster and all have relatively high amplitude. Every other flux measurement, of any star in the cluster, will be divided by the reference curve. This is done to determine how it varies compared to the reference stars. The result of the division is a light curve of each target star where now the relative flux is plotted against time. Since this curve is expected to be a straight line with little to no fluctuations, it is much easier to identify flux variations that is not caused by noise, a transiting exoplanet for example.

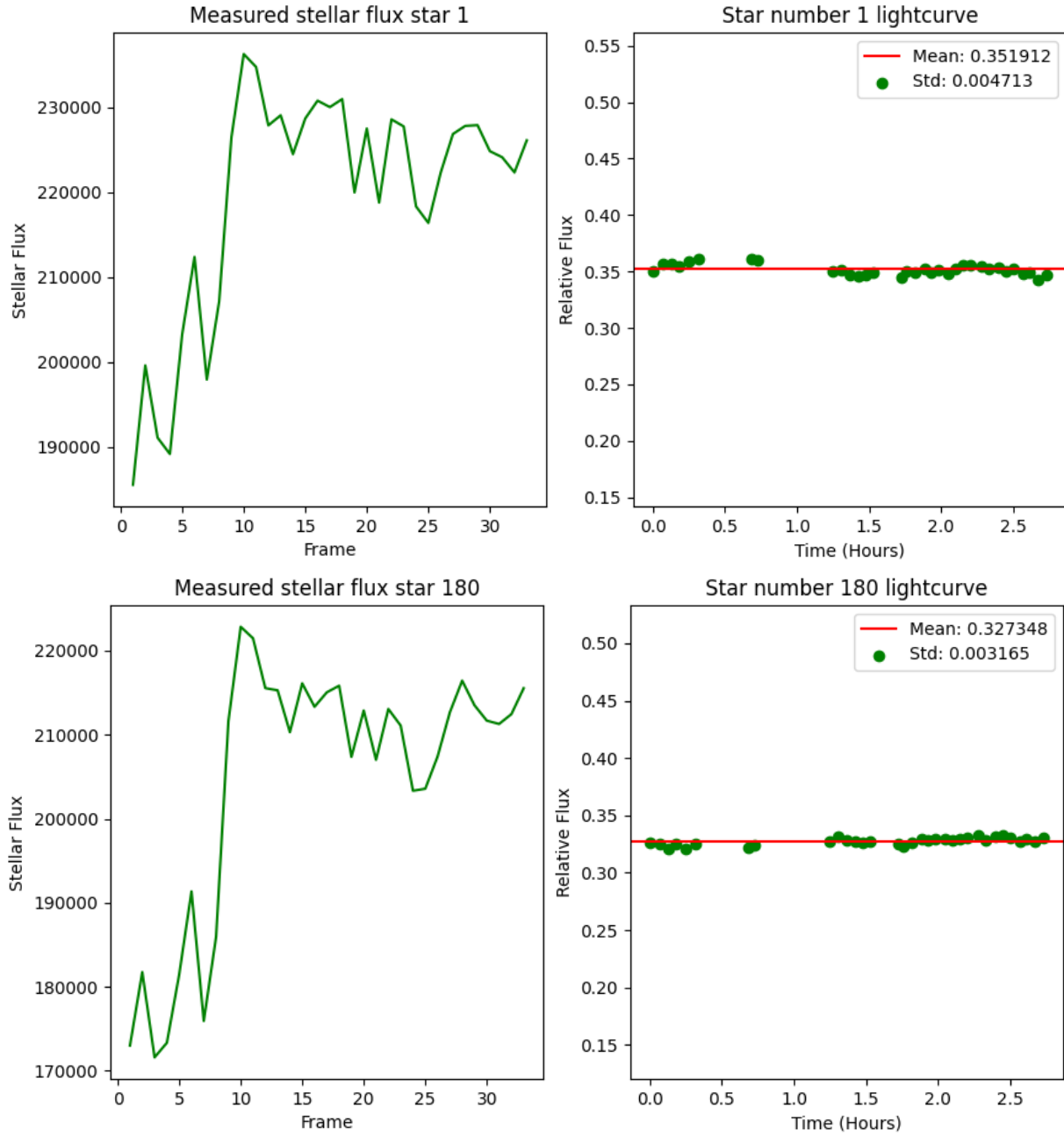


Figure 2.14: Measured stellar fluxes of stars numbered 1 and 180 and the corresponding light curve.

As said, bias and dark frames was taken at random times during the observation and is why the light curves in figure 2.14 have no data at times  $0.32 \text{ h} < t < 0.68 \text{ h}$ ,  $0.73 \text{ h} < t < 1.25 \text{ h}$  and  $1.53 \text{ h} < t < 1.72 \text{ h}$ .

# Chapter 3

## Data analysis

Doyal "Al" Harper, professor at University of Chicago, Astronomy and Astrophysics division, observed the M3 GC with  $g$  and  $r$  filters using the StoneEdge 0.5m telescope. The observations took place 27th and 28th of January 2023 with the purpose to obtain data that could be used for education. I obtained the  $g$  and  $r$  filter images from the Stone Edge database and performed noise reduction on them in the same way as described in the beginning of this chapter. The  $g$  and  $r$  filter images were used to create an HR-diagram, in order to identify the stellar types of the stars identified in the science images obtained during my observation 1st February. Ideally, the same stars identified from my observation should be identified in the  $g$  and  $r$ -filter images as well. To do this, positions of the stars in the  $g$  and  $r$  images were predicted with help of the science images. By using the tracking strategy, the tracking star was found in the filtered images and the shift between all 3 images was calculated. This shift was added onto all the stars found in my images to predict the position of the same stars in the  $g$  and  $r$  filter images. The flux of the stars in the  $g$  and  $r$  images were calculated by fitting 2D Gaussians using the same strategy as for when calculating the flux of the stars in the science images. The fluxes was then used to calculate the apparent magnitudes using the formula below.

$$m_s - m_{ref} = -2.5 \log_{10} \frac{F_s}{F_{ref}}$$

Using the flux of the star,  $F_s$ , and the flux of the reference star,  $F_{ref}$ , to calculate the apparent flux.  $m_s$  and  $m_{ref}$  is the apparent magnitudes of the star and reference star respectively. The reference star was chosen to be the same as the tracking star, number 9, since it is very bright and well isolated. The calculated magnitude values of the stars in the  $g$  filter image was then plotted against the value of  $(g-r)$ , that is the magnitude of the star in the  $g$  filter subtracted by the magnitude of the same star in  $r$  filter, to obtain the HR-diagram.

Depending on the stars positions in the HR-diagram, different stellar radii could be derived where I assigned the brighter stars larger radii and the fainter smaller. Because of the age of M3, that is 11.4 Gy, the sub-giant branch consists of stars with radii between





In this project, the transit depth that a  $1R_j$  sized HJ would produce will be compared to the noise in the light curve. This was calculated using equation 1.1. By calculating the ratio between the standard deviation and the transit depth, reveal if a transit is readily visible in the light curve or not.

$$\frac{\sigma}{\left(\frac{R_p}{R_*}\right)^2} > 1 \implies \text{Transit not readily visible in the light curve}$$

$$\frac{\sigma}{\left(\frac{R_p}{R_*}\right)^2} \leq 1 \implies \text{Transit readily visible in the light curve}$$

Looking at the center image in figure 3.2, it is clear that something went wrong with the 9th measurement as it deviates very much from the other values. In some of the lightcurves, one or more of these "faulty measurements" could be found and they contributed to errors as the mean and standard deviation was calculated using faulty data. Because of that, if a measurement differ more than a set threshold value from both of its neighboring measurements, it is considered a bad measurement and is set to not be included when calculating the mean and standard deviation.

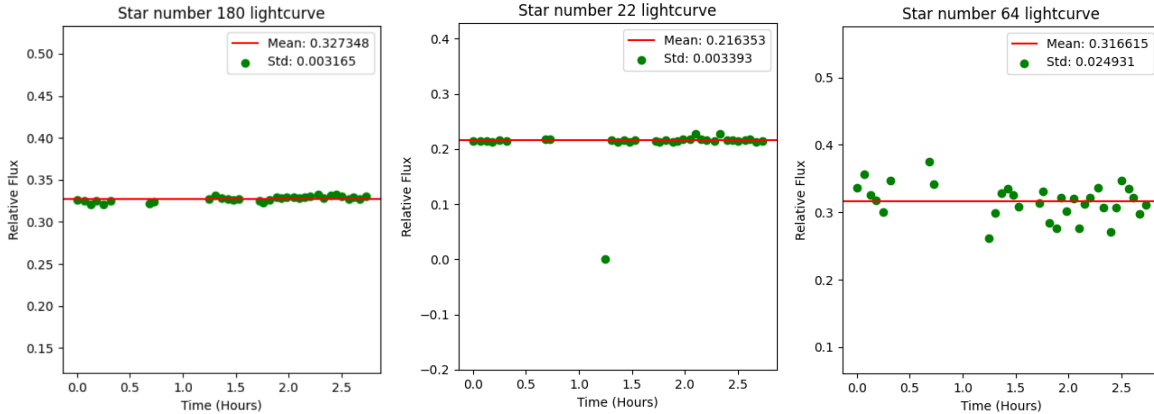


Figure 3.2: The left image display a lightcurve without any bad measurements. The middle and left image are examples of lightcurves containing bad measurements. Middle image have one bad measurement. The one measurement is ignored when calculating mean and standard deviation. In the right image, the code identified 16 bad measurements. Thus even if the measurements are ignored in further calculations, a transit would not be detectable either way, hence the lightcurve is considered a bad measurement. Images obtained from the code.

Further, if more than 4 of the measurements are considered bad measurements, the whole series is considered unreliable and is marked as a "bad measurement" light curve. The reason for faulty measurements could be that it did not find an optimised fit

to the star in one of the frames due to, as an example, two stars are positioned very close to each other and the optimizer fails to identify them as two separate stars. In some of the images, some stars became elongated which could also lead to the optimizer not identifying the star as an actual star. The elongation is likely due to field distortion, caused by the image magnification not being homogeneous over the entire lens. This can cause objects in the outer parts of the image to appear elongated or misshaped <sup>1</sup>.

---

<sup>1</sup><https://web.archive.org/web/20090129134205/http://toothwalker.org/optics/distortion.html>

# Chapter 4

## Results

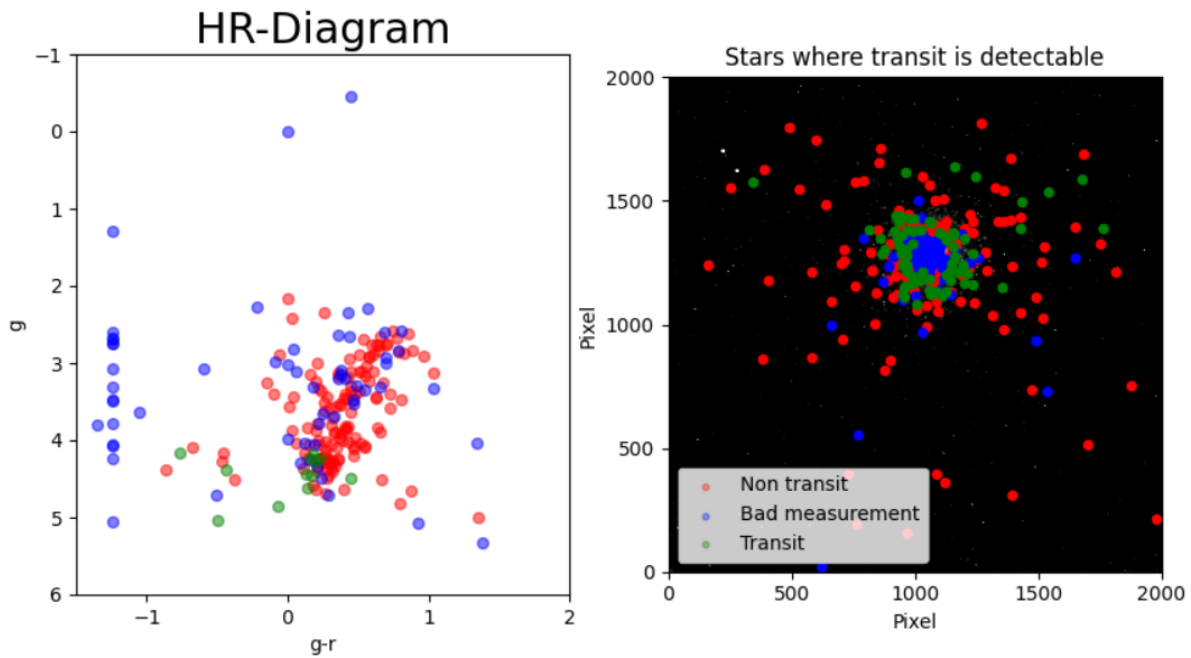


Figure 4.1: The result of the transit search. Left image is the same HR-diagram displayed in figure 3.1 but stars are now colored green (transit detectable), red (non-transit) or blue (bad measurement). Right image display where the stars are positioned.

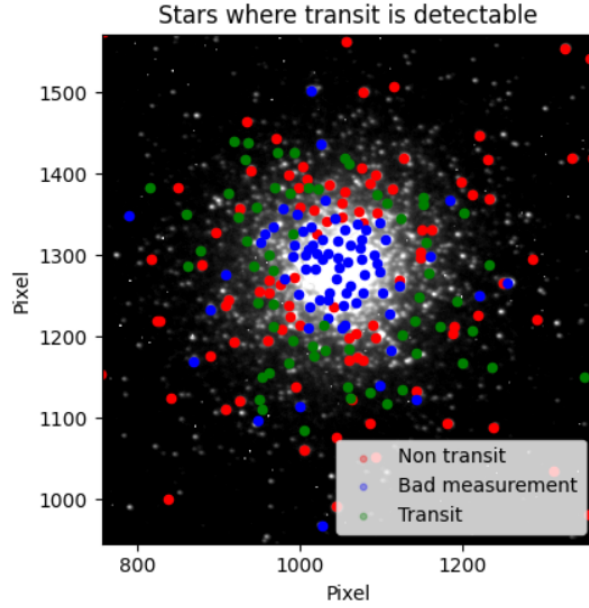


Figure 4.2: An enhancement of the left image in figure 4.1, showing the center of the cluster more clearly.

Star Radius ( $R_{\odot}$ )	Type	Total of Stars	Transit Visible (%)	No transit visible (%)	Bad Measurements (%)
6	Giant	37	0	67.5	32.5
5	Giant	45	0	73.3	26.7
4	Giant	32	0	84.4	15.6
3	Giant	65	13.8	70.8	15.4
2	Subgiant	9	33.3	55.5	11.1
1	Main Sequence	65	90.7	6.2	3.1
<b>Failed HR-measurement</b>	-	37	0	0	100
<b>Total</b>	-	290	24.5	48.3	27.2

Table 4.1: Table showing statistics of different stellar radii, displaying the percentage of transits, non transits and bad measurements. The row "Failed HR-measurements" contains failed color-measurements. Thus, they were never given a radii and further excluded from the transit search.

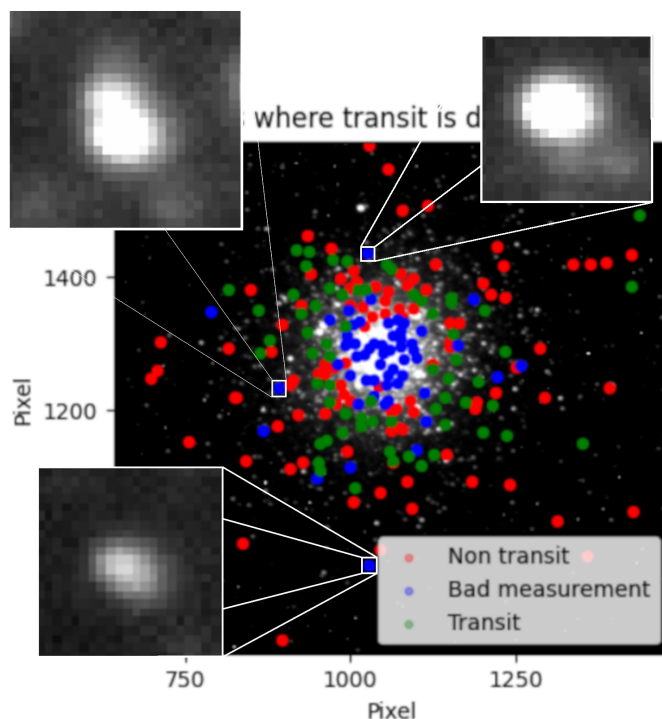


Figure 4.3: Image showcasing 3 stars outside the center of the cluster which still produced bad measurements.

## 4.1 Discussion

The observations with the Stone Edge observatory during the 1st of February gave very clear science images in the sense that a lot of stars around the center of the GC are easy to distinguish and at the same time having high pixel count values without being over exposed. This is also the case after the image reduction where, as displayed in figure 2.3, a lot of the noise is removed in the outer parts of the cluster but also as the center is approached. In figure 2.3 it can clearly be seen that the radius of the uniformly bright area has decreased, resulting in an increase of how many stars could be distinguished closer to the center by StarfinderDAO.

When it comes to fitting the stars, the Gaussian fitting method was very reliable. As can be seen in figure 2.10, gaussians are fitted very accurately in both position and shape of the stars in the sub image. However problems arose when stars were placed very close to each other and the optimizer identified two (or more) separate stars as one. This effect is seen in figure 2.11, where the star finder correctly identify three individual stars but the optimizer finds them as the same. Although this problem was solved in the outer regions of the cluster by placing a limitation on the optimizer, it caused for some errors as the center was approached. In the center, no individual stars could be distinguished which was caused by the optimizer not finding the optimized values within the

limitations, resulting in a lot of measurements where no star was actually found, which is why we see the number of bad measurements increase as the center is approached. However, it is likely that many of the measurements inside the cluster would have been unreliable even if the limitations had not been set, since it would have increased the risk of measurements looking similar to figure 2.11. But over all, the code manage to correctly fit most of the stars individually in the outer regions of the cluster where the light is not homogeneous.

The HR-diagram could be used to exclude some non-members. A trend can clearly be seen and it is comparable to the giant branch seen in figure 1.5. However the number of stars included in the HR-diagram has to be increased to be able to more clearly be able to identify the stellar type of the stars. The stars between 194-225 in the HR-diagram are much fainter stars and was added manually with the goal of trying to distinguish the turn off and main sequence stars as well. Unfortunately, the stars in the  $g$ -filter image was very faint and only 30 more stars were able to be correctly identified and fitted in both the  $r$  and  $g$  filter images. This could be fixed by capturing the color images with a higher exposure time or by stacking multiple images onto each other, as that would mean more light would have been captured. However the result of the 30 added stars produced what is interpreted as the Subgiant branch seen at  $-1 < x < 0$ . It was then assumed that all of the stars that are visible in the science images but not in the  $g$  filter, has to be turn off/main sequence stars with stellar radius equal or less than the solar radius. Since they can not be plotted in the HR-diagram, it was not possible to arrange the MS stars into different stellar radii. Because of this, it is possible that some of the MS stars actually have smaller radii than what is stated. However, this would just cause for even more and deeper transits and would thus increase the number of transits found rather than decrease. On the other hand, because the MS stars are not plotted in the HR-diagram, I can not know that they all actually are MS stars. It is possible that the reason they appear fainter is because they are background stars located further back in the cluster, meaning a transit would maybe not be visible if it was placed at an equal distance as the other stars. But looking at figure 1.5 it is clear that the cluster is home to a lot of MS stars that are not plotted in my HR-diagram. Thus my assumption that the fainter stars are MS stars can not be that far off. Similarly, there are some stars that are located in the foreground. As an example, the tracking star, star number 9, is believed to be a foreground star because of its very bright appearance. In the HR-diagram, two stars are seen at  $g < 0$  that is star number 9 and 10. Although they were not identified as bad measurements in the filtered images, it is clear that they differ a lot from the other stars in the diagram. This is probably the case for some other stars in the diagram as well, as some stars are seen to deviate more or less from the trend in the HR-diagram which would contribute to faulty assumptions about their radius, affecting the result.

The results presented in figure 4.2 and table 4.1 are more or less what was expected. Observing the center of the cluster gave nothing but bad measurements where stars are not distinguished correctly or the flux measurements deviates very much from each

other, producing light curves representing more or less random scattered points. However, a cut off point can be seen around the center where the vast majority of stars are actually producing accurate measurements. The reason they would not produce a visible transit is only due to the planet being very small and not being able to produce a transit depth big enough to be observed, however that does not imply that the strategy of observing them have failed. Some bad measurements can still be seen outside the cluster and the reason for this is showcased in figure 4.3. The two stars on the top in figure 4.3 have one or more stars positioned very close to the star of interest. Due to the series being 33 frames long, it is possible that in some frames the stars are being fitted differently. As an example, in one frame the all stars are identified separately, while in the other frames they are all identified as one star. Due to this, the calculated flux can have very different values from one frame to another which the code will identify as bad measurements. The star on the bottom is seen to be elongated. Usually this is not a problem for the Gaussian fitting of the star, however if stars get too elongated the StarfinderDAO will fail to identify it as a star. This means that it will not fit a Gaussian to it and further no flux measurement will be made and the frame is marked as a bad measurement.

As seen in table 4.1, the number of detected transits increase as the stellar radii decrease which is exactly what is expected since the transit depth will become deeper. This is also clearly visible from the colored HR-diagram in figure 4.1, as transits are only seen on the sub-giant branch. Similarly, the amount of bad measurements decreases rapidly with decreasing stellar radii. This can be interpreted as that stars with larger radii are located more to the center of the cluster. That may be reasonable, since we see an increase of stars as the center is approached. Due to the stellar density increasing, more giants will be seen there as well as many other stars.

The telescope is probably the main reason for the amount of bad measurements. A bigger telescope equipped with a higher resolution camera that is able to resolve stars located at smaller angular distances from each other, would decrease the area of the homogeneous circle of light which has the greatest bad measurement density. Also, to detect a planetary transit around sub-giant stars one will have to produce light curves with way less noise in order to detect a flux decrease caused by a HJ with  $1R_J$ .

Although no real exoplanets were found in this project, my results would also point towards a possible absence of them. By simply using a larger telescope and observing the cluster for a longer time, planets at some distance from the center could have been detected in previous transit searches, such as in R.L.Gilliland et al.(2000) and J.J.Wallace et al.(2020) work. Thus if I would be able to observe a transit with my setup, so would Gilliland and Wallace.

## 4.2 Conclusion & Outlook

Using my method, telescope and strategy a transit search in the M3 globular cluster would produce accurate light curves on 72.8% of the identified stars. The remaining 27.2% are stars located close to the center of the cluster, where distinguishing individual stars is not possible with the observational setup that was used. In 33.6% of the accurate light curves, a HJ with radius equal to one Jupiter radius would be detectable. This is mainly because of the size of the stars, since the vast majority of the transit-detectable stars are main sequence stars with radius equal to the Sun. Hence a transit is seen around these stars mainly because of the ratio between planetary radius and stellar radius is greater which results in a deeper transit depth. If globular clusters are home to exoplanets, we have the greatest possibility of detecting them around MS stars at some distance from the center.

If this project were to be continued with, the first improvement would be to use a larger telescope such that more stars in the cluster can be individually distinguished. I would also have wanted to observe for a longer period of time. Since even if a planet are present around any of the stars that was observed, due to the relatively short observation time, periodic flux decreases will never be visible. I would also like to do real simulations of planetary transits around the stars to be able to obtain more reliable data, rather than just comparing the theoretical transit depth with the noise. The color images need some improvement to become more reliable. By setting a longer exposure time on both the  $g$  and  $r$  filter would increase the number of stars included in the survey which would result in clearer relationships between transit, stellar position and type. Although the code to obtain light curves is very fast, I would like to improve it by making it fully automatic. In this version, the desired star will have to be manually asked for. This is because for some stars the initial parameters will have to be manually changed such that the right star is found and fitted nicely. With more time, I would modify the code such that if it is given a set of coordinates to  $X$  number of stars, it would automatically iterate through the entire set without me manually asking it to do calculations for every individual star. My coding ability was limited when the project started and it has increased a lot throughout the project. Thus with more time, I would also like to rewrite my code to make it even more efficient than it is right now, by maybe using different packages or different strategies to approach problems in a different way.



# Bibliography

- Chattopadhyay, T., Mondal, S., Paul, S., Maji, S., & Kumar Chattopadhyay, A. 2021, *ApJ*, 911, 22
- Gilliland, R. L., Brown, T. M., Guhathakurta, P., et al. 2000, *ApJ*, 545, L47
- Hamers, A. S. & Tremaine, S. 2017, *AJ*, 154, 272
- Higgins, M. E. & Bell, K. J. 2023, *AJ*, 165, 141
- King, I. 1962, *AJ*, 67, 471
- Laughlin, G. 2000, *ApJ*, 545, 1064
- Masuda, K. & Winn, J. N. 2017, *AJ*, 153, 187
- McLean, I. S. 2008, *Electronic imaging in astronomy* (Praxis Publishing Ltd)
- National Academies of Sciences, E. & Medicine. 2018, *Exoplanet Science Strategy* (Washington, DC: The National Academies Press), 150
- Pols, O. R., Schröder, K.-P., Hurley, J. R., Tout, C. A., & Eggleton, P. P. 1998, *MNRAS*, 298, 525
- Wallace, J. J., Hartman, J. D., & Bakos, G. Á. 2020, *AJ*, 159, 106